

# Cell Migration on Cell-Internalizable Ligand Microdepots: A Phenomenological Model

JANE S. TJIA and PRABHAS V. MOGHE

Department of Chemical and Biochemical Engineering, Rutgers University, Piscataway, NJ

(Received 17 August 2001; accepted 9 April 2002)

**Abstract**—We have shown that collagen “ligand associated microdepots” (LAMs) at polymer substrates can significantly enhance levels of skin epidermal cell migration (Tjia and Moghe, *Tissue Eng.* 8:247–259, 2002). In this study, we have further examined the dynamics of cell–LAM interactions, primarily through a phenomenological model to examine the differential effects of LAM–cell binding and LAM internalization within the cells. Based on the experimental data of cell migration and LAM dynamics under selected conditions, the model was solved to yield rates of LAM binding and internalization at various LAM substrate densities. The clearance dynamics of LAMs computed at various times from the model matched well with the LAM clearance kinetics observed experimentally. The model was used to generate simulations of the rates of LAM binding and internalization over time, under conditions of differential exogenous activation. Our model analysis suggests that the rate of cell migration can be sensitively governed by rate of cellular sampling of LAMs, given by differential rates of LAM binding and internalization. Maximal cell migration was found to occur during LAM presentation regimes (LAM spatial density) that engendered concerted changes in the extent of cell activation, as measured via net tyrosine kinase activity, due to LAM sampling dynamics. © 2002 Biomedical Engineering Society. [DOI: 10.1114/1.1492814]

**Keywords**—Cell migration; Ligand microengineering; Receptor-mediated cell endocytosis; Nanoparticles; Microparticles.

## INTRODUCTION

Cellular migration is a coordinated process that results from the interaction of specific cell surface receptors with ligands of the extracellular matrix (ECM).<sup>25</sup> Using well-controlled, stable, ligand substrates, a number of ligand properties have been shown to affect activation of cell motility, including, for example, ligand surface concentration, strength of ligand–receptor adhesion, degree of receptor occupancy by the ligand, and ligand affinity.<sup>23</sup> Recently, the ligand microdistribution on biomaterial surfaces has also been shown to modulate the

valency of receptor–ligand binding, with effects on cell spreading.<sup>20</sup> Ligand microinterfaces that exhibit more complex, dynamic, cell interactions can also be envisioned: for example, those that elicit receptor-mediated cell binding and adhesion, but also activate cell signaling through active substrate internalization, through a process called phagocytosis.<sup>1</sup> Such interfaces occur frequently *in vivo*, when cells contact a ligand-presenting surface and migrate on it through ligand internalization, a process called phagokinetic migration.<sup>7</sup> For example, during wound healing, skin epidermal cells called keratinocytes have been shown to phagocytose ECM ligand debris that lie directly in their migratory path. The design of phagokinesis promoting ligand interfaces may thus be of value to the development of tissue scaffold configurations that promote the kinetics of scaffold coverage or cell infiltration.<sup>4,16</sup>

However, the parameters regulating phagokinetically coupled cell migration have not been systematically investigated. Previously, we have experimentally demonstrated the use of dynamic, ligand-adsorbed microcarriers, which, when internalized by cells, can elicit significantly enhanced extent of migration over that observed on substrate-adsorbed ligand substrates [Figs. 1(a) and 1(b)].<sup>33</sup> These studies were done using colloidal gold microdepots adsorbed with the adhesion ligand, collagen. The ligand-adsorbed microdepots (LAMs) were coated onto collagen–PLGA substrates such that the total ligand density and the amount of ligand per microcarrier were kept constant [Fig. 1(c)]. We showed that the rate of cell migration exhibited was strongly dependent on the LAM substrate density [Fig. 2(a)], and that the cell–LAM interactions essential for enhanced migration were ligand-activated, as motility was significantly reduced in the absence of ligands on the microcarriers [Fig. 2(b)]. Moreover, cell migration could be severely repressed when cell internalization processes were blocked via covalent attachment of the microcarriers to the underlying substrate, indicating that the signals from cell–LAM binding alone were insufficient for increased migration [Fig. 2(b)]. Finally, the analysis of the cell–substrate

Address correspondence to Professor Prabhas Moghe, Department of Biomedical Engineering; Department of Chemical and Biochemical Engineering, Rutgers University, 98 Brett Road, Piscataway, NJ 08854. Electronic mail: moghe@rci.rutgers.edu

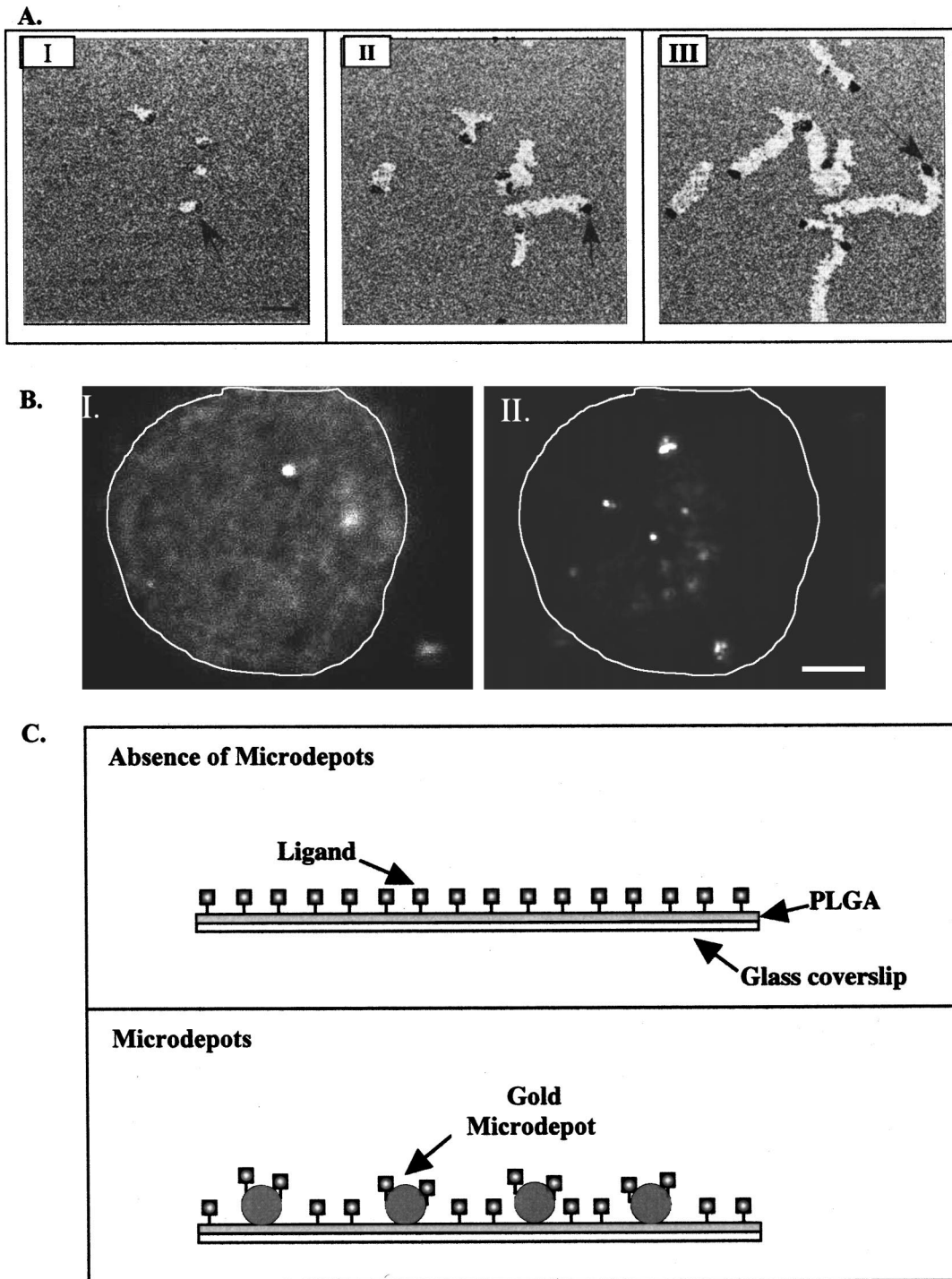


**FIGURE 1.** Migration of keratinocytes on ligand-bound microdepots. (A) Representative micrographs of keratinocyte clearance in the presence of ligand microcarriers at  $1.21 \text{ LAMs}/\mu\text{m}^2$ . As the keratinocytes migrate, they leave behind areas cleared of LAMs (arrows). Representative images are shown at 0 h (I), 2.5 h (II), and 5 h (III). Bar =  $50 \mu\text{m}$ . (B) Representative confocal images of intracellular LAM internalization. Cells were allowed to migrate on substrates containing LAMs for 30 min prior to fixation and staining with Dil. Confocal fluorescent sections ( $0.5 \mu\text{m}$ ) were then obtained in order to determine the cell boundaries, (I). Reflected confocal sections were obtained to visualize internalized LAMs (II). Combining the two images, it was possible to determine the extent of LAM internalization. Representative confocal sections are shown for a cell that has been allowed to migrate and ingest LAMs on a substrate containing  $0.345 \text{ LAMs}/\mu\text{m}^2$ . Bar =  $10 \mu\text{m}$ . (C) Schematic illustration of ligand-bound microdepot-coated substrates. Collagen ligands were adsorbed onto PLGA-coated coverslips in the presence or absence of ligand microdepots such that the overall surface concentration of the ligand was constant. Soluble FN was added as an exogenous stimulus in selected conditions and is not diagrammed here.

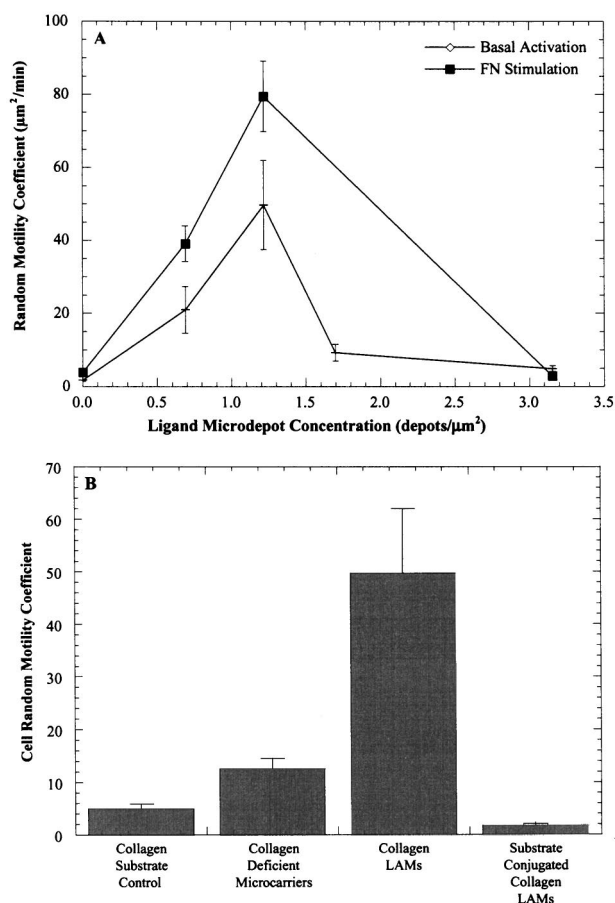


**FIGURE 2.** Effect of ligand microdepot concentration on the cell random motility coefficient. (A) Estimates of the random motility coefficient were obtained as previously described as a function of the initial ligand microdepot density. For each depot concentration, 40–50 cells were analyzed. (B) Estimates of the random motility coefficient were also obtained in the absence or presence of collagen on the microdepots and when internalization was inhibited by covalent attachment of the microdepots to the substrate. For these experiments, a microdepot substrate density of 1.21 microdepots/ $\mu\text{m}^2$  was used. The error bars represent the standard error.

adhesivity suggested that activation changes elicited via LAM density were primarily manifested at the cell–LAM interface, rather than at the cell–substrate interface. However, the rate processes underlying cell–LAM interactions have not yet been analyzed.

In this study, we formulated a simple model of the major cell–LAM interactions during the induction of keratinocyte motility on collagen-associated microcarriers, under two different modes of activation elicited with or without a soluble exogenous activator, fibronectin.<sup>32</sup> Based on the experimental studies of cell migration and specific processes underlying cell–LAM interaction, including cell–LAM binding and internalization, the model was solved to obtain the rates of LAM binding and internalization at various LAM substrate densities over

time. Our studies suggest that for a given rate of cell motility, there appears to be a correlation between the rate of cell migration and the rates of LAM “sampling,” the differential of rates of LAM binding and internalization. Further, the model formalism can be applied to elucidate how ligand microcarrier presentation dynamics affects the extent of net cell activation as measured by net tyrosine kinase activity.

## EXPERIMENTAL METHODS

### Cell Culture

Human keratinocytes from neonatal foreskin were isolated by enzyme digestion<sup>31</sup> and cultured in serum-free keratinocyte growth medium (KGM) (Clonetics, San Diego, CA) containing 0.1 ng/mL epidermal growth factor (EGF), 5  $\mu\text{g}/\text{mL}$  insulin, 0.5  $\mu\text{g}/\text{mL}$  hydrocortisone, 50  $\mu\text{g}/\text{mL}$  gentamicin, 50 ng/mL amphotericin-B, 0.15 mM calcium, and 30  $\mu\text{g}/\text{mL}$  bovine pituitary extract (BPE). Keratinocyte isolations were screened for contaminating fibroblasts using indirect immunofluorescence staining for keratin 14 and vimentin (Sigma, St. Louis, MO). In all experiments, cells were used at passage 2 or 3. To fully define the culture media for experiments, media was switched to KGM without BPE and EGF 6 h prior to the initiation of the experiment.

### Substrate Preparation

Glass coverslips (25 mm diam) were cleaned using soap and sonication and stored in 100% ethanol until use. As previously described, thin polymer films were obtained by spincoating a 1% w/v solution of 50:50 poly D,L (lactic acid-glycolic acid) (PLGA) (Medisorb, Cincinnati, OH) in chloroform onto cleaned coverslips. PLGA films were then coated with type-I rat tail collagen (Collaborative, Bedford, MA) at a concentration of 5  $\mu\text{g}/\text{cm}^2$  by slowly evaporating 1 mL of a 24.2  $\mu\text{g}/\text{mL}$  collagen solution in 0.2N acetic acid at room temperature. The substrates were then placed in six well plates and held in place with a small amount of silicone glue.

Prepared substrates were next coated with collagen-adsorbed particulate gold salts in order to stimulate phagocytosis. Gold salts were prepared as previously described.<sup>1</sup> Briefly, 11 mL of distilled water was combined with 6 mL of 36.5 mM  $\text{Na}_2\text{CO}_3$  and 1.8 mL of 14.5 mM  $\text{AuCl}_4\text{H}$  (J.T. Baker, Phillipsburg, NJ). The solution was heated just to boiling and 1.8 mL of a 0.1% formaldehyde solution was added. In order to prevent any substrate denaturation, the solution was then cooled to below 70 °C. The cooled solution was layered over the prepared substrates (2 mL) and incubated at room temperature for 45 min. The addition of the gold solution at these temperatures results in desorption of a significant portion of the collagen. The collagen then binds to the

gold particles through noncovalent interactions. In some experiments, substrates were coated with a solution made without AuCl<sub>4</sub>H prior to the addition of gold particle solution to obtain final substrates with nonligand adsorbed microparticles. We have previously shown that substrates prepared in this manner contain a final collagen concentration of 612 ng/cm<sup>2</sup>.<sup>32</sup>

In order to decrease the surface particle concentration, the coating solution was diluted. To increase the surface concentration, the total amount of gold solution layered over the substrates was increased. Previous studies have shown that gold particles formed in this manner are monodisperse with an average diameter of approximately 400 nm.<sup>2</sup> In order to verify the final surface particle concentration, transmitted microscopy images of the substrate surface were obtained at 100× magnification and analyzed using image analysis. In experiments where no gold particulates were used, substrates were coated with a solution made without AuCl<sub>4</sub>H.

#### *Time Lapse Microscopy and Image Analysis of Cell Migration*

Keratinocytes were plated onto prepared substrates in six well plates in KGM media without BPE at a density of 2000 cells/cm<sup>2</sup> and allowed to attach for 2 h at 37 °C. Thirty ng/mL of EGF (Sigma, St. Louis, MO) was simultaneously added with the cells. In some experiments, soluble fibronectin stimulation was incorporated by adding 10 μg/mL fibronectin (Sigma, St. Louis, MO) to the media. After the attachment period, the six well plates were transferred to the motorized, heated stage of a Zeiss Axiovert laser scanning microscope (Zeiss, Inc., Thornwood, NY). The microscope stage was kept at 37 °C using a customized stage incubator. All cell tracking was performed under bright field at 10× magnification with 1.5× zoom. Using LSM 410 software (Zeiss, Inc., Thornwood, NY), a macro was written to store and track three representative fields of view from each coverslip in the six well plates. Scanned images were obtained every 3 min up to a total time of 5 h. Images were then processed using Image-Pro software (Media Cybernetics, Silver Spring, MD) to analyze the paths of the individual migrating cells. Between 5 and 12 cells were analyzed in each field of view. Only cells whose paths did not intersect those of other cells over the migration period were selected for analysis. Selected cells were highlighted and their centroids at each time point recorded. In addition, the area cleared by the cells at each time point was also determined.

#### *Determination of Random Motility Coefficient, μ*

The random cell motility coefficient was determined using the formulation originally proposed by Dunn,<sup>12</sup> and later by Othmer *et al.*<sup>28</sup> Briefly, the random motility of

individual cells was characterized by regression of the mean-squared displacement behavior of the cell population as function of time:

$$\langle d^2(t) \rangle = 4\mu[t - P(1 - e^{-t/P})], \quad (1)$$

where  $\langle d^2(t) \rangle$  is the mean-squared displacement,  $P$  is the cell directional persistence time, and  $t$  is the time interval of the experiment. Using the  $(x, y)$  coordinates of the cell centroids, squared displacements were calculated to be

$$d^2(t) = (x_{t+\Delta t} - x_t)^2 + (y_{t+\Delta t} - y_t)^2. \quad (2)$$

In order to take advantage of all positional data available, overlapping intervals were used. Mean-squared displacements were calculated at given time intervals and fit to Eq. (1) using the Levenberg–Marquardt nonlinear least-squares regression algorithm to obtain estimates for  $\mu$  and  $P$ .

#### *Determination of Net Tyrosine Kinase Activity*

The activation state of migrating cells was quantified via the determination of tyrosine kinase activity. Substrates containing various densities of ligand-adsorbed microdeposits were prepared as previously described<sup>33</sup> on 25 mm diam coverslips and placed in six well plates. Primary keratinocytes isolated from neonatal foreskin and cultured in serum-free medium<sup>32</sup> were then seeded at a density of 1E4 cells/cm<sup>2</sup> and allowed to attach and migrate for 2 h at 37 °C. Cells were then lysed with 150 μL M-Per mammalian protein extraction agent (Pierce, Rockford, IL) containing 10 μg/mL leupeptin, 40 μg/mL pepstatin A, 200 μM PMSF, and 100 μM sodium orthovanadate (all from Sigma, St. Louis, MO). Collected cell lysates were kept at −20 °C until time of assay. Tyrosine kinase activity was determined using a nonradioactive tyrosine kinase assay kit (Roche Molecular Biochemicals, Indianapolis, IN) and normalized to the activity of cells seeded on substrates without LAMs.

## MATHEMATICAL FORMULATION

### *Phagocytosis*

The dynamics of the LAM uptake process were examined from a kinetic–mechanistic point of view in which the cell–LAM interaction events were modeled using equations similar to those used in traditional Michaelis–Menten kinetics. In order for a LAM to be ingested, molecules on the microcarrier surface must first interact and bind with receptors, lectins, or other molecules on the cell surface. We hypothesize that this initial particle binding, while triggering the phagocytic process, however, is not sufficient for particle ingestion. Further

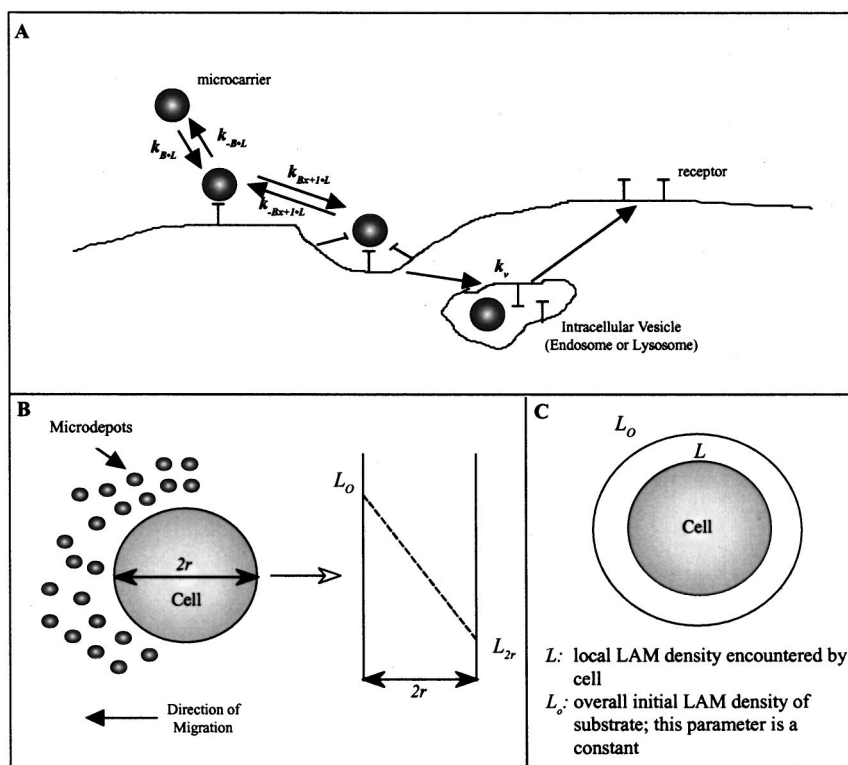
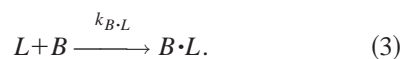


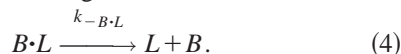
**FIGURE 3.** Schematic of proposed model (A) dynamics of cell-LAM interactions. Microdepots initially bind to one cell membrane/surface receptor. Before they can be internalized, additional membrane/receptors must be recruited in order to “activate” the depot for internalization. Once internalized, the depot dissociates from the membrane/receptor and the membrane/receptor gets recycled back to the cell surface. (B) Contribution of migration to model: analogy to diffusion across a semi-infinite plane. (C) Cells encounter a local LAM density,  $L$ , as they migrate, which can differ from the initial overall LAM density of the system,  $L_o$ .

sequential recruitment of cell surface receptors into interactions with the remainder of the particle surface is assumed to be necessary.<sup>17–19</sup> These receptor–ligand interactions control the advancement of the pseudopodial extension of the plasma membrane, which is engulfing the particle. Thus, if there are not sufficient receptors on the cell surface or ligands on the particle surface to allow engulfment of the particle, phagocytosis will not proceed. This is the dominant mechanism by which phagocytosis is believed to occur and has been termed the “zipper” model.<sup>29</sup> In addition, previous studies have shown that there is a positive correlation between the rate of ECM-coated latex beads ingested and the number of ECM molecules per bead,<sup>21,27</sup> providing further evidence of the multivalent nature of ECM receptor binding required for optimum phagocytic ingestion. In keeping with the zipper model, the mechanism behind the LAM uptake process is proposed to proceed by the following sequence of elementary reactions, as shown in Fig. 3(a):

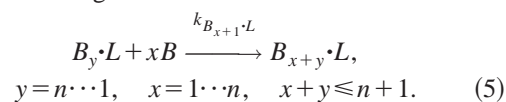
- (1) A ligand-adsorbed microcarrier,  $L$ , binds to a cell-microcarrier binding site,  $B$ , to form a LAM-binding site complex,  $B \cdot L$ :



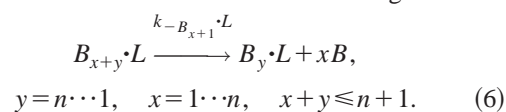
- (2) This complex can decompose back to an unbound particle and free-binding site:



- (3) Or, if there is a sufficient number of free-binding sites available, it can bind to  $x$  more binding sites to form an “activated” particle-binding site complex capable of being ingested. The value of  $x$  may be any number between 1 and  $n$ , the number of additional binding sites needed to form a fully activated complex. Thus, a series of reactions may take place of the following form:

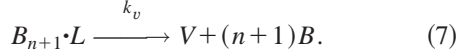


- (4) Like the inactivated form, the activated complex and all of its intermediates, can decompose back to previous inactivated forms and  $x$  free binding sites:



- (5) Once the particle-binding site complex becomes fully activated, it can be ingested by the cell to form an intracellular vesicle,  $V$ . Within the vesicle, the particle becomes uncoupled from the binding sites and the now free binding sites are recycled to the cell surface. For the purposes of our model, we lump the rates of ingestion and binding site recycling into

one parameter,  $k_v$ :



In addition, for the time course of our experiments, the expression level of the cell, or the total number of binding sites, is assumed to be constant and is given by the following expression:

$$B_T = B + \sum_{x=0}^n [(x+1)B_{x+1} \cdot L]. \quad (8)$$

### Cellular Migration

Cell migration will affect the degree of exposure of LAMs to the cell, as migration would make new LAMs available for internalization. Previous studies have shown that in isotropic environments, migrating cells can be characterized as exhibiting a persistent random walk.<sup>12,28</sup> This behavior indicates that they move along fairly linear paths over short periods of time, but show more randomly oriented paths over longer time intervals. A population of cells exhibiting this behavior can be characterized primarily in terms of  $\mu$ , the random motility coefficient, while single cells exhibiting random motility are typically characterized by  $S$ , cell speed, and  $P$ , persistence time.<sup>15</sup> The population-derived random motility coefficient has been shown to be linked to the single cell parameters of cell speed and persistence time via the equation  $\mu = 1/2 S^2 P$  and, studies have confirmed that values of cell speed calculated from population migrations agree well with those calculated from single cell parameters.<sup>14</sup> Because  $\mu$  incorporates both cell speed and persistence time, it gives an inherently more complete description of cell motility than either cell speed or persistence time alone. In our system, as a first approximation, the overall density of LAMs,  $L_o$ , is assumed to be uniform and isotropic. Over relatively short times, the local binding and depletion of LAMs may bias the directionality of cell migration; however, over longer time periods, the mean-squared displacement of migrating cells as a function of time reaches linearity. Thus, we make use of the persistent random walk theory and use  $\mu$  as the primary parameter characterizing migration in our system.

In order to determine the contribution of cellular migration to cell-LAM dynamics, we make an analogy to molecular diffusion in a semi-infinite plane [Fig. 3(b)]. Consider an inverse system in which the cells are stationary and the LAMs are motile, with a constant random motility coefficient,  $\mu$ . We make the assumption that the cell is well spread and can be modeled as a flat plane. While a large portion of LAMs will become bound to the cell at the cell's leading edge, some LAMs

will remain on the substrate surface as the cell moves over them and only encounter a free LAM binding site further along the cell membrane. Therefore, the mass balance of extracellular LAMs encountered locally by the cell is given in terms of the local LAM concentration,  $L$  [Fig. 3(c)]:

$$\frac{d}{dt}(A_{\text{cell}}L) = 2rj_{2r}, \quad (9)$$

where  $A_{\text{cell}}$  is the spread area of the cell,  $r$  is the cell radius, and  $j$  is the LAM flux across a cell of diameter  $2r$ . The flux across a semi-infinite plane is

$$j_z = \frac{\mu}{z}(L_o - L_z), \quad (10)$$

where  $z$  is the characteristic length of the cell. In our analysis, we take  $z$  to be the cell diameter,  $2r$ . Assuming that the area of the cell is much greater than that of the particle, we can assume that there are very few extracellular LAMs at  $z = 2r$ , thus,  $L_z = 0$ . Substituting Eq. (10) into Eq. (9), we obtain an expression relating the rate of cell migration to the rate of change of the extracellular local LAM concentration:

$$\frac{d[L]}{dt} \text{Migration} = \frac{\mu L_o}{\pi r^2} = \frac{\mu L_o}{A_{\text{cell}}}. \quad (11)$$

### Composite Model

Using Eqs. (3)–(11), we next formulate the following kinetic expressions that comprise the composite model. In defining these expressions, we make the inherent assumption that free ligands (ligands not adsorbed onto microcarriers) do not contribute significantly to the extent of migration relative to the contribution of LAMs.

- (1) Rate of change of the concentration of local extracellular LAMs,  $L$ , encountered by the cell:

$$\frac{d[L]}{dt} = -k_{B \cdot L}[L][B] + k_{-B \cdot L}[B \cdot L] + \frac{\mu L_o}{A_{\text{cell}}}. \quad (12)$$

- (2) Rate of change of the concentration of initial LAM-binding site complexes,  $B \cdot L$ :

$$\begin{aligned} \frac{d[B \cdot L]}{dt} &= k_{B \cdot L}[L][B] - k_{-B \cdot L}[B \cdot L] \\ &\quad - \sum_{y=1}^n \sum_{x=1}^n k_{B_{x+y} \cdot L}[B_{y \cdot L}][B]^x \\ &\quad + \sum_{y=1}^n \sum_{x=1}^n k_{-B_{x+y} \cdot L}[B_{x+y} \cdot L]. \end{aligned} \quad (13)$$

- (3) Rate of change of the concentration of partially “ac-

tivated” LAM-binding site complexes,  $B_{x+1}\cdot L$ :

$$\begin{aligned} \frac{d[B_{x+y}\cdot L]}{dt} = & \sum_{y=1}^{n-1} \sum_{x=1}^{n-1} k_{B_{x+y}\cdot L}[B_y\cdot L][B]^x \\ & - \sum_{y=1}^{n-1} \sum_{x=1}^{n-1} k_{-B_{x+y}\cdot L}[B_{x+y}\cdot L]. \end{aligned} \quad (14)$$

(4) Rate of change of the concentration of fully “activated” LAM-binding site complexes,  $B_{n+1}\cdot L$ :

$$\begin{aligned} \frac{d[B_{n+1}\cdot L]}{dt} = & k_{B_{n+1}\cdot L}[B\cdot L][B]^n - k_{-B_{n+1}\cdot L}[B_{n+1}\cdot L] \\ & - k_V[B_{n+1}\cdot L]. \end{aligned} \quad (15)$$

(5) Rate of change of the concentration of internalized LAMs,  $V$ :

$$\frac{d[V]}{dt} = k_V[B_{n+1}\cdot L]. \quad (16)$$

The net effects of cell migration were experimentally measured in terms of the rate at which cells effectively “clear” an area covered with ingestible LAMs. For a given initial surface particle concentration, the area of LAM clearance by a cell is equal to the sum of the number of particles bound and ingested, divided by the initial particle concentration:

$$\frac{d(\text{cleared\_area})}{dt} = \frac{1}{L_o} \left[ \sum_{x=0}^n \frac{d[B_{x+1}\cdot L]}{dt} + \frac{d[V]}{dt} \right]. \quad (17)$$

Equations (12)–(17) thus define the mathematical model equations for the effect of phagocytosis on cellular migration.

## MODEL ANALYSIS

Analysis of the model was performed for two activation conditions: activation with 30 ng/mL soluble EGF only (basal activation), and activation with both 10  $\mu\text{g/mL}$  soluble fibronectin and 30 ng/mL EGF (fibronectin stimulation).

### Case 1: Basal Activation

In order to solve the model under conditions of basal activation, several simplifying assumptions were made. Previous experimental results<sup>32</sup> have shown that in the presence of particulate matter, migrating cells will completely clear a path through the particles, leaving few free particles behind. Therefore, we assume that the rate of inactivated LAM-binding site complex decomposition,  $k_{-B\cdot L}$ , is very small compared to the rate of initial binding,  $k_{B\cdot L}$ , and can be neglected. In addition, it is

assumed that the fully activated complex,  $B_2\cdot L$ , once formed, is highly reactive and is quickly ingested. Thus, this complex would be present only in low concentrations and may be assumed to be at pseudosteady state.

As will be described in the following section, the value of  $n$ , the additional integer number of binding site equivalents needed for activation, was calculated to be 1 under basal activation conditions. Since it is difficult to differentiate between binding site–LAM complexes that are inactivated or activated, we combine the two complexes to obtain total bound LAMs. However, since the concentration of the activated complex is assumed to be small, the majority of the bound LAMs will be present in the inactivated complex form:

$$\frac{d[\text{Bound}]}{dt} = \frac{d[B\cdot L]}{dt} + \frac{d[B_2\cdot L]}{dt} \approx \frac{d[B\cdot L]}{dt}. \quad (18)$$

Taking into account the above assumptions, we obtain the following simplified mathematical model system:

$$\frac{d[L]}{dt} = -k_{B\cdot L}[L][B_T - B\cdot L] + \frac{\mu L_o}{A_{\text{cell}}}, \quad (19)$$

$$\frac{d(B\cdot L)}{dt} = k_{B\cdot L}[L][B_T - B\cdot L] - k_V \left[ \frac{(B_T - B\cdot L)(B\cdot L)}{K_m + 2(B\cdot L)} \right], \quad (20)$$

$$\frac{d[V]}{dt} = k_V \left[ \frac{(B_T - B\cdot L)(B\cdot L)}{K_m + 2(B\cdot L)} \right], \quad (21)$$

$$\frac{d(\text{clearance})}{dt} = \frac{1}{L_o} \left( \frac{d[B\cdot L]}{dt} + \frac{d[V]}{dt} \right), \quad (22)$$

where

$$K_m = \frac{k_{-B_2\cdot L} + k_V}{k_{B_2\cdot L}}. \quad (23)$$

### Case 2: Fibronectin Stimulation

For an  $n$  value of 2, the following model reactions can take place:

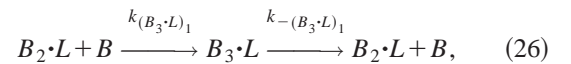
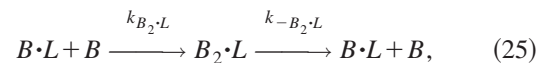
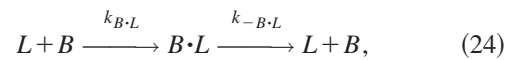
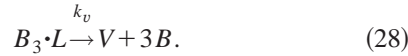
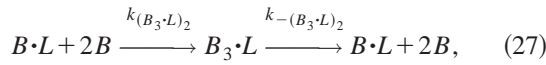


**TABLE 1. Experimentally determined model parameters.** Model parameters were determined from experimental results. Values of the LAM binding capacity of the cell,  $B_T$ , were determined from the number of bound LAMs in the presence of excess LAM density. Knowing  $B_T$ , and the average cell diameter, the additional number of binding sites needed for activation,  $n$  was then calculated. The kinetic constant of binding,  $k_{B,L}$ , was determined from the slope of a plot of the initial number of bound LAMs as a function of the initial LAM density. The kinetic constant of internalization,  $k_v$ , was determined from a Lineweaver–Burk Plot.  $K_m$  is a parameter that combines the kinetic constants found in Eqs. (11)–(13) and was also determined from a Lineweaver–Burk Plot. The parameter  $a$  is a constant whose value depends on the parameter  $n$ , the additional number of binding sites needed for activation.

	Parameter	Basal activation	Fibronectin stimulation
$B_T$	Total number of binding sites	12,708 particles	20,170 particles
$n$	Additional number of binding sites	1	2
$k_{B,L}$	Kinetic constant of cell–LAM binding	2.06E-3 $\mu\text{m}^2/\text{particle min}$	1.52E-3 $\mu\text{m}^2/\text{particle min}$
$k_v$	Kinetic constant of LAM internalization	1.28E-3 $\text{min}^{-1}$	2.40E-3 $\text{min}^{-1}$
$K_m$	Kinetic constant of LAM activation (critical site equivalents, $a$ )	0.7295 particles/ $\mu\text{m}^2$ ( $a \sim 2$ )	0.5012 particles/ $\mu\text{m}^2$ ( $a \sim 3$ )



As in the case for basal activation, the rate of decomposition of the initial particle–binding site complex,  $k_{-B \cdot L}$ , is assumed to be negligible compared to the rate of initial binding and can be neglected. In addition, it is probable that a much greater concentration of the fully activated complex,  $B_3 \cdot L$ , will be formed through a combination of Eqs. (25) and (26) than from Eq. (27) alone. Thus, we assume that the reaction represented in Eq. (27) does not occur to a large extent and its contribution to the model can be neglected. We also disregard the rates of decomposition of the partially activated complex,  $B_2 \cdot L$ , and the fully activated complex,  $B_3 \cdot L$ , under the assumption that they are much slower than the rates of formation. Finally, as in the previous case, we assume that the concentrations of the fully activated complex,  $B_3 \cdot L$ , as well as the partially activated intermediate complex,  $B_2 \cdot L$ , are very small compared to the concentration of the initial complex,  $B \cdot L$ , and can be assumed to be a steady state. With these assumptions, the model equations take the form:

$$\frac{d[L]}{dt} = -k_{B \cdot L}[L][B_T - B \cdot L] + \frac{\mu L_o}{A_{\text{cell}}}, \quad (29)$$

$$\frac{d[B \cdot L]}{dt} = k_{B \cdot L}[L][B_T - B \cdot L] - \frac{k_v[B \cdot L][B_T - B \cdot L]}{K_m + 3[B \cdot L]}, \quad (30)$$

$$\frac{d[V]}{dt} = \frac{k_v[B \cdot L][B_T - B \cdot L]}{K_m + 3[B \cdot L]}, \quad (31)$$

where

$$K_m = \frac{k_v}{k_{B_2 \cdot L}}, \quad (32)$$

and

$$\frac{d[\text{Bound}]}{dt} = \frac{d[B \cdot L]}{dt} + \frac{d[B_2 \cdot L]}{dt} + \frac{d[B_3 \cdot L]}{dt} \approx \frac{d[B \cdot L]}{dt}, \quad (33)$$

$$\frac{d(\text{clearance})}{dt} = \frac{1}{L_o} \left( \frac{d[B \cdot L]}{dt} + \frac{d[V]}{dt} \right). \quad (34)$$

Analysis of the above systems of equations was performed using an explicit Runge–Kutta method in Matlab (The Mathworks, Inc., Natick, MA) and to provide clearance profiles under varying conditions of soluble stimulation and at varying initial LAM densities. In addition to clearance profiles, the temporal rates of LAM binding and internalization, along with the net LAM sampling rate were determined at various initial LAM densities.

## RESULTS

### Determination of Model Parameters

Calculated model parameters are shown in Table I.

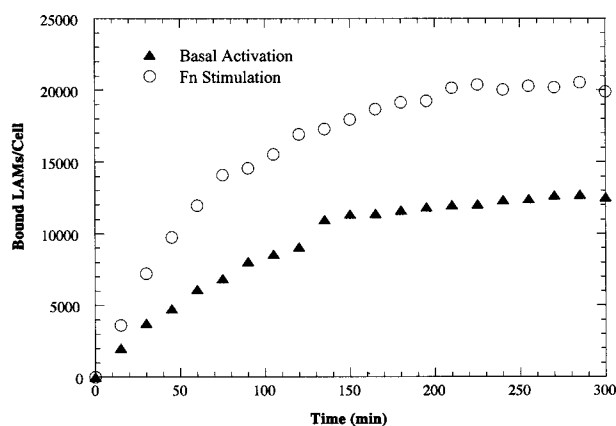


**FIGURE 4.** Determination of the total number of binding sites,  $B_T$ . Plot of the number of LAMs bound per cell as a function of time for cells migrating on substrates containing an excess amount of LAMs ( $4.61 \text{ LAMs}/\mu\text{m}^2$ ). The number of LAMs at which saturation was reached was found to be 12,708 LAMs under basal conditions, and 20,170 LAMs under fibronectin stimulation conditions.

*Total Number of Binding Sites,  $B_T$ .* The total number of binding sites,  $B_T$ , was assumed to be equivalent to the maximum number of LAMs that could bind to a cell. Experiments were performed in which cells were allowed to migrate on substrates containing an excess amount of LAMs ( $4.61 \text{ LAMs}/\mu\text{m}^2$ ). Under these conditions, it was assumed that the majority of the area cleared was due to initial LAM binding to the cell surface and not to LAM activation or ingestion. The number of LAMs bound per cell was thus plotted as a function of time until saturation was reached and the total number of bound LAMs was taken to correspond to the total number of LAM binding sites (Fig. 4).

*Additional Number of Binding Sites,  $n$ .* The parameter  $n$  represents the number of additional binding sites with which the initially bound LAM must form interactions in order to be ingested. Although it is difficult to determine the exact number of binding sites needed, it is possible to approximate the area of plasma membrane necessary to fully engulf a LAM. The average diameter of cells during the experiments (84 cells measured over seven experiments) was found to be  $37.95 \pm 0.85 \mu\text{m}$ . Since it is difficult to determine the exact degree of cell spreading, we examine the two possible extremes and take the average. If the cell is completely spread, it can be approximated as a thin disk, with surface area  $2\pi r^2 = 2262.27 \pm 105.94 \mu\text{m}^2$ . The area is doubled to account for both the upper and lower faces of the cell. If the cell is fully rounded, the surface area is  $4\pi r^2 = 4524.53 \pm 211.88 \mu\text{m}^2$ . The average surface area is therefore  $3393.40 \pm 158.91 \mu\text{m}^2$ . The average diameter of the gold particles has previously been found to be  $0.4 \mu\text{m}$  with a surface area of  $0.51 \mu\text{m}^2$ .<sup>2</sup> Based on the total number of

LAM binding sites per cell, the average area of plasma membrane bound to each particle and the approximate amount of additional membrane needed to fully engulf the LAM could be determined. An approximate integral value of  $n$  could thus be calculated from the following formula:

$$|n| = B_T \frac{SA_{\text{LAM}}}{SA_{\text{cell}}} - 1. \quad (35)$$

For example, the total number of binding sites per cell under basal activation conditions was found to be 12,707.8 sites. Dividing the average surface area of a cell,  $3393.40 \mu\text{m}^2$ , by the total number of binding sites, 12,707.8 results in each LAM initially binding to approximately  $0.268 \mu\text{m}^2$  of cell membrane. Since  $0.51 \mu\text{m}^2$  are needed to fully engulf the membrane, the amount of membrane per cell would need to approximately double (integral multiples) before the LAM could be ingested. Thus, in our model the value of  $n$  under basal activation conditions is taken to be 1.

*Kinetic Constant of Binding,  $k_{B \cdot L}$ .* Estimates for  $k_{B \cdot L}$ , the kinetic constant for the initial cell–LAM binding reaction, were obtained by sparsely seeding cells onto substrates containing a known LAM concentration and incubating the samples for 1 h. Three images at each LAM concentration were then obtained using brightfield microscopy at  $20\times$ . The area cleared by single cells was then determined using Image-Pro software and averaged. Knowing the initial LAM concentration and the area cleared, the number of LAMs that had effectively been cleared from the surface was calculated. At the early time point employed, it was assumed that minimal cellular migration had occurred, few LAMs had been bound, and a large majority of the cell binding sites was still unoccupied. Thus, Eq. (12) reduces to

$$\frac{d[L]}{dt} = -k_{B \cdot L}[B_T][L_o]. \quad (36)$$

A plot of  $dL/dt$  vs  $B_T L_o$  should fit to a line with slope  $-k_{B \cdot L}$  and intercept 0 (Fig. 5). Between 30 and 40 cells were analyzed at each particle concentration.

*Kinetic Constant of Ingestion,  $k_v$ , and  $K_m$ .* As shown in the previous section, assumptions used in the analysis of the model result in Eqs. (13)–(15) collapsing into one equation of the general form:

$$\frac{d[V]}{dt} = k_v \left[ \frac{(B_T - B \cdot L)(B \cdot L)}{K_m + a(B \cdot L)} \right], \quad (37)$$

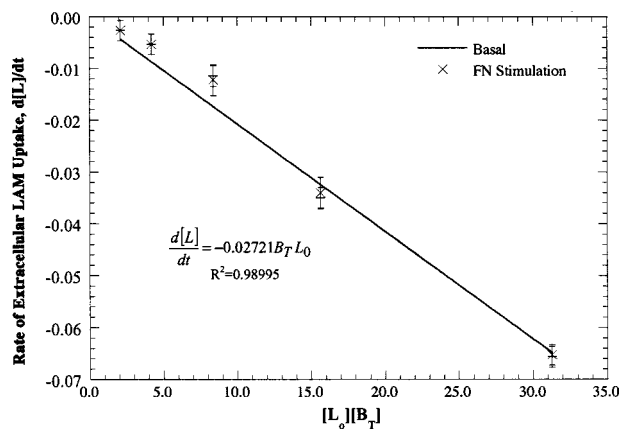


FIGURE 5. Determination of the kinetic constant of binding,  $k_{B-L}$ . Estimates for the kinetic constant of binding,  $k_{B-L}$  were obtained using Eq. (20). A plot of  $dL/dt$  vs  $B_T L_0$  yields a line with slope  $-k_{B-L}$  and intercept 0. Linear curve fits resulted in  $R^2$  correlation coefficients of 0.98995 for both basal and fibronectin activation conditions.

where  $a$  is equal to the total number of binding sites needed for LAM engulfment,  $n+1$ .  $K_m$  is a term that combines the kinetic constants in Eqs. (16)–(18) and its exact definition is also dependent upon the value of  $n$ . Estimates for  $k_v$  and  $K_m$  were obtained using a slight modification of a Lineweaver–Burk plot. Rearranging and taking the inverse of Eq. (37):

$$\frac{(B_T - B \cdot L)}{dV/dt} = \frac{K_m}{k_v} \left( \frac{1}{B \cdot L} \right) + \frac{a}{k_v}. \quad (38)$$

A plot of  $(B_T - B \cdot L)/(dV/dt)$  vs  $1/(B \cdot L)$  yields slope of  $K_m/k_v$  and intercept  $a/k_v$  (Fig. 6). Immunofluorescence confocal microscopy in conjunction with reflected confocal microscopy was used to obtain values for the rate of ingestion,  $dV/dt$ . Sparsely seeded cells were allowed to migrate on substrates containing varying surface particle concentrations. After 30 min, cells were incubated for an additional 10 min at 37 °C with 1  $\mu\text{m}$  DiI (Molecular Probes, OR). Cells were then trypsinized, fixed, and plated on glass slides for viewing under confocal microscopy. Using reflected confocal microscopy, optical sections of the cell were taken in 0.5  $\mu\text{m}$  increments. Under reflected light, the ingested LAMs appear white against a black background. The membrane dye, DiI, was used to determine the cell boundaries under fluorescent confocal microscopy. Using both fluorescent and reflected confocal images, the number of particles ingested by a single cell could be determined. The concentration of bound particles at specific initial particle concentrations was known from experiments to determine  $k_{B-L}$ .

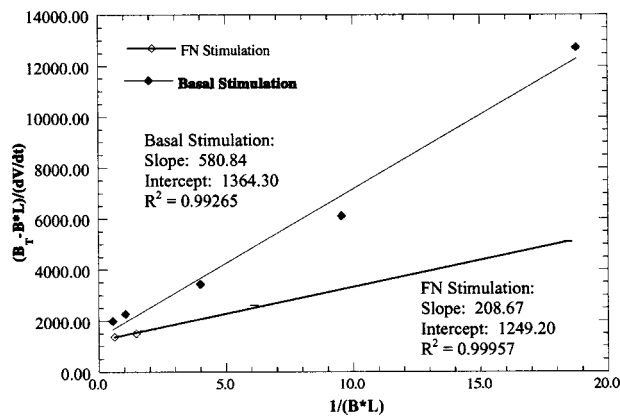
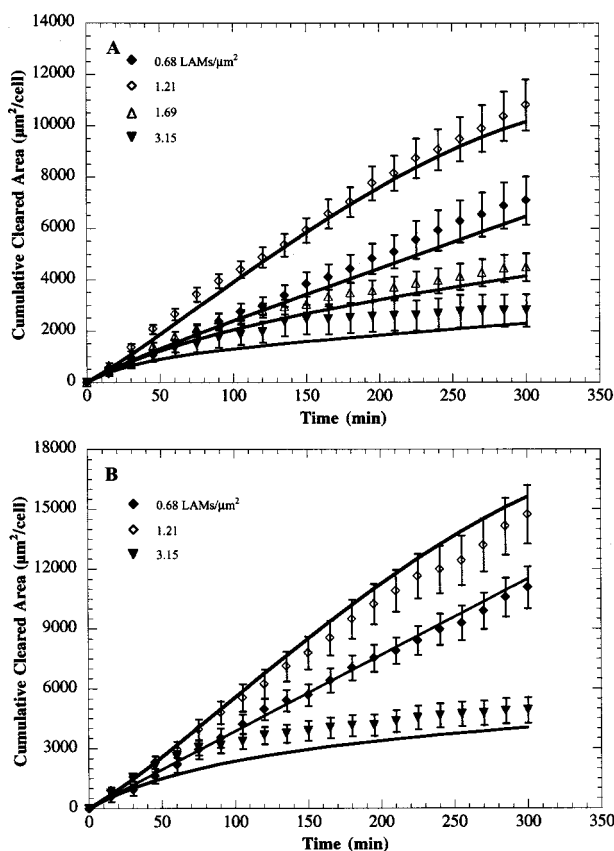


FIGURE 6. Determination of the kinetic constant of ingestion,  $k_v$ , and  $K_m$ . Estimates for  $k_v$  and  $K_m$  were obtained using a slight modification of a Lineweaver–Burk plot as described in Eq. (21). A plot of  $(B_T - B \cdot L)/(dV/dt)$  vs  $1/(B \cdot L)$  yields slope of  $K_m/k_v$  and intercept  $a/k_v$ . Linear curve fits resulted in  $R^2$  correlation coefficients of 0.99265 and 0.99957 for basal and fibronectin activation conditions, respectively.

#### Model Validation

In order to validate the model, simulations of migratory clearance were compared to previous experimental results<sup>33</sup> (Fig. 7). Briefly, keratinocytes were sparsely seeded onto prepared substrates containing ligand-coated LAMs at various densities and monitored using time-lapse microscopy. In general, theoretical values of cumulative cleared area were found to exhibit similar trends to those found experimentally. At lower LAM concentrations, the cumulative cleared area was found to steadily increase at a relatively constant rate. As the LAM concentration increased above the optimum value, the rate of clearance was found to decrease. Simulation results revealed good agreement with experimental points at LAM concentrations of 0.688 and 1.21 LAMs/ $\mu\text{m}^2$ . At these initial LAM concentrations, theoretical values were found to be within 10% of experimental results. However, at higher LAM concentrations, model simulations consistently under-predicted the cumulative cleared area. At 1.68 LAMs/ $\mu\text{m}^2$ , theoretical values deviated from experimental results by an average of 16.27%. Increasing the LAM concentration to 3.15 LAMs/ $\mu\text{m}^2$  increased the amount of deviation to 26.52%. Stimulation with soluble fibronectin at 3.15 particles/ $\mu\text{m}^2$  resulted in an average deviation of 25.77% [Fig. 4(b)].

The results of the model accurately predict the level of migratory activity expected at low surface LAM concentrations. However, predictions at higher LAM concentrations were consistently lower than experimental results. This underestimation may be attributed mainly to the high degree of particle “agglomeration” observed at higher LAM concentrations (leading to multivalent binding, which is not accounted for in the strictly binary



**FIGURE 7. Effect of LAM internalization on cleared area.** Theoretical simulation results of cumulative cleared area at various LAM densities were compared to previous experimental results (Ref. 33) under conditions of (A) basal activation and (B) fibronectin stimulation. Theoretical simulation results are denoted by the solid lines and were obtained by simultaneously solving Eqs. (19)–(22) (for the basal case) and Eqs. (29)–(34) (for fibronectin stimulation) using Matlab.

interactions of the model), and in part, to the assumptions made in determining  $k_{B-L}$ , the kinetic constant of binding. Most significantly, it was assumed that at the early time point, a majority of the cell–LAM binding sites were still unoccupied. While this assumption may have been valid at low LAM concentrations, the greater rate of initial LAM binding expected at higher concentrations might have led to an underestimation of  $k_{B-L}$  at those initial conditions.

One of the major simplifications of the model is its restriction that all kinetic constants be time invariant. It is possible that as time progresses, the overall rate of LAM ingestion may be limited by the amount of free-binding sites. However, it has previously been found that phagocytic cells can vigorously recruit intracellular membranes to the cell surface during phagocytosis.<sup>5</sup> Thus, it is quite likely that the cells may have compensated for the loss of binding sites by recruiting internal membranes to the plasma membrane, effectively increasing their capacity to bind new LAMs. Additionally, be-

cause it was difficult to decouple the rate of “replenishment” of the binding sites in our system, the rates of binding site ingestion and recycling were implicitly lumped together while determining the rate of LAM ingestion (implying that receptor/membrane recycling is not a rate-limiting step). In the future, data for receptor/membrane recycling would need to be factored in to improve the model accuracy, particularly for conditions of higher LAM concentration and longer time incubations.

Another simplification of the model is the assumption made regarding cell spreading in the calculation of  $n$ , the integral number of critical binding sites. Previous studies regarding cell spreading and migration have shown that the cell migration rate can be inversely related to the cell spread area,<sup>34</sup> suggesting the role for dynamic limitations arising from membrane availability. However, if a cell is too rounded and not adequately spread, the cell cannot gain enough traction on the surface it can push or pull against.<sup>11</sup> It appears, therefore, that there is an optimum degree of spreading at which a cell is able to migrate effectively without membrane limitations. The exact degree of membrane spreading that is considered optimal, however, has not been established and is likely to vary depending upon the cell type, as well as the ligand properties. Thus, in our calculations for  $n$ , we averaged the cell area based on the two possible extreme configurations of cell spreading (a completely spread cell and a completely rounded cell). Slight variations in cell spreading, however, may lead to significant variations in the cell surface area, that may, in turn, lead to errors in the estimation of the value for  $n$  and, subsequently,  $k_v$ . Based on our calculations, we found that the value of  $n$  under basal activation conditions could range from  $2.18 \pm 0.16$  to  $0.59 \pm 0.08$  based on the extreme values of cell spreading. Corresponding values of  $k_v$  range from  $2.33E-3$  to  $1.17E-3 \text{ min}^{-1}$ . Overestimations of  $k_v$  may lead to overestimations of LAM binding, as faster internalization would lead to a faster recycling of binding sites. However, given that model simulation results do not overpredict LAM clearance under any of our test conditions, overestimates of  $k_v$  may not play a significant role in our model simulations. On the other hand, underestimating  $k_v$  could result in an underestimation of clearance, particularly at higher LAM substrate densities, where the availability of LAM binding sites is limiting. Future experiments aimed at determining the exact number of available receptors on the cell surface coupled to a known display of ligands on each LAM would facilitate more robust estimates for  $n$ .

#### *Effect of LAM Spatial Density on the Cell–LAM Binding and Internalization Rates*

Using the mathematical model developed, the effects of the initial LAM substrate density on the rate of cell–

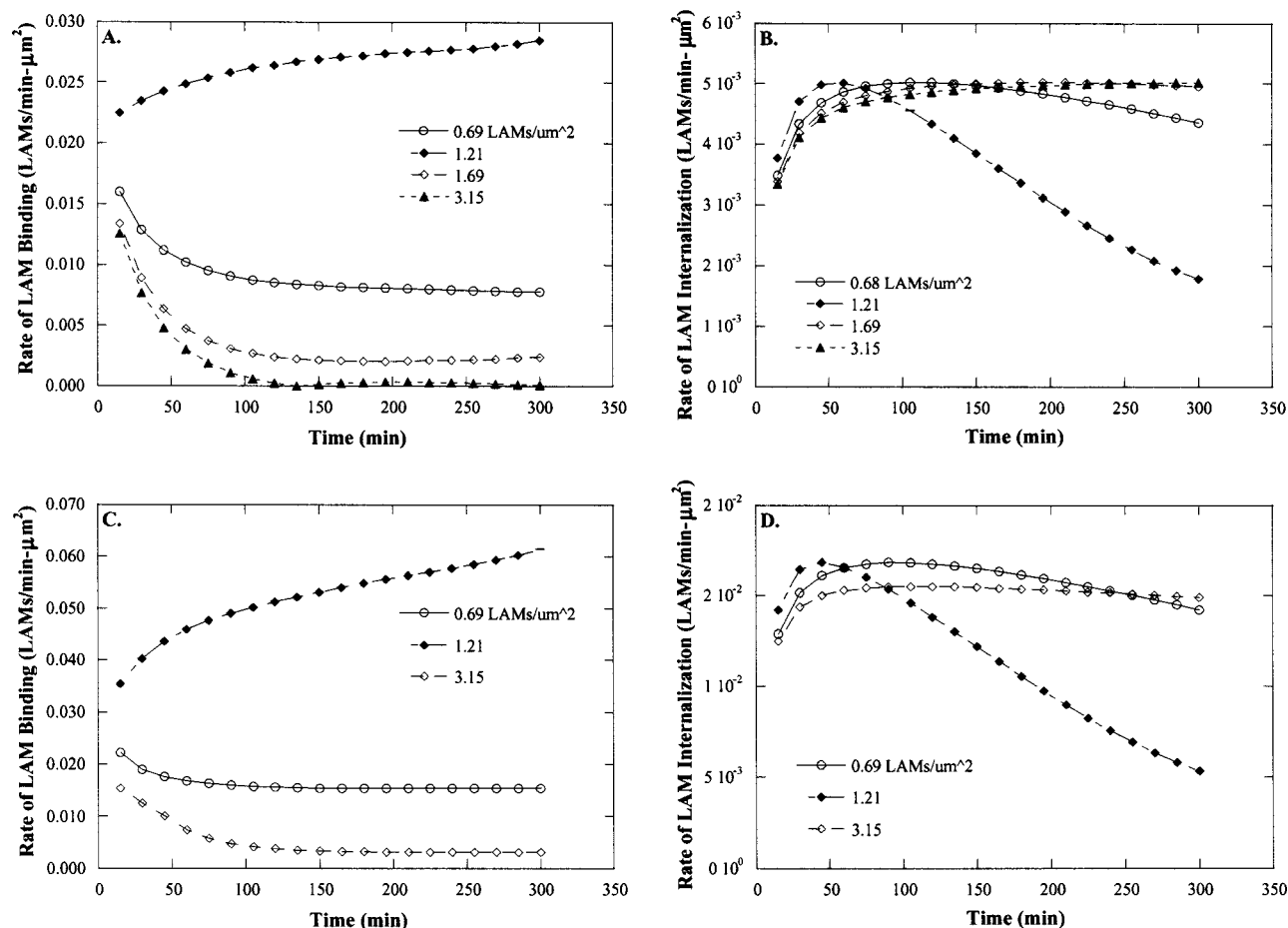


FIGURE 8. Theoretical temporal evolution of LAM binding and internalization rates. The model was used to generate average LAM binding (A) and (C) and LAM internalization (B) and (D) rates as a function of time for various initial LAM densities. Results were obtained for both basal (A) and (B) and fibronectin (C) and (D) stimulation conditions.

LAM binding and internalization were simulated over a 5 h period. The initial rate of LAM binding was found to exhibit a biphasic dependence on the substrate LAM density, with the highest initial rate of binding occurring at 1.21 LAMs/ $\mu\text{m}^2$  [Fig. 8(a)]. Regardless of the substrate density, however, the rate of LAM binding quickly reached a steady state, the level of which depended on the initial LAM density.

Analysis of the rate of LAM internalization showed that it was significantly slower than the rate of LAM binding [Fig. 8(b)]. Moreover, there was initially no effect of substrate LAM density on internalization rates. However, as time progressed, the rate of internalization was found to steadily decrease at 1.21 LAMs/ $\mu\text{m}^2$ . A slower decline was also observed at 0.68 LAMs/ $\mu\text{m}^2$  with minimal changes seen at 1.69 and 3.15 LAMs/ $\mu\text{m}^2$ . Further analysis showed a positive correlation between the calculated equilibrium net LAM sampling rate (LAM binding rate *minus* LAM internalization rate) and the experimentally determined cell random motility coefficient, with fibronectin-stimulated conditions exhibiting

similar correlations as those elicited under basal activation conditions (Fig. 9).

#### *Effect of Cell–LAM Interactions on Tyrosine Kinase Activity*

The tyrosine kinase activity of migrating cells on various LAM substrate densities was determined using a nonradioactive tyrosine kinase activity assay and normalized to the activity of cells seeded on substrates without LAMs. In order to discern the contribution of LAM binding versus internalization to the extent of cellular activations, the relative tyrosine kinase activity was plotted as a function of the LAM binding rate [Fig. 10(a)] and as a function of the LAM internalization rate at constant initial binding rate [Fig. 10(b)]. Examination of tyrosine kinase activity as a function of LAM binding revealed similar trends as those observed as function of the net sampling rate, with a slight decrease as the net sampling rate increased. Increasing activity was observed as the internalization rate increased.

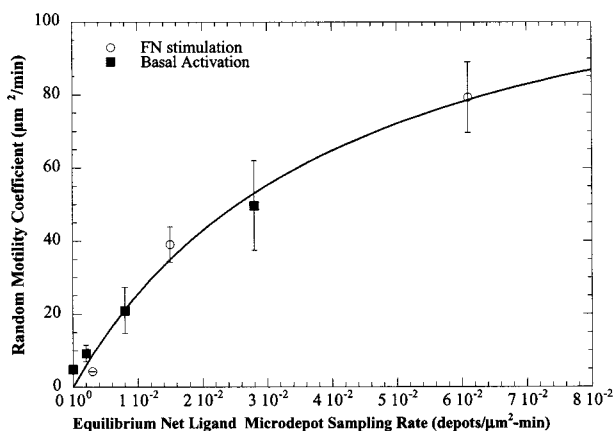


**FIGURE 9.** Theoretical relation between random motility coefficient and net ligand microdepot sampling rate. Analysis of the model shows that the theoretically determined net rate of microdepot binding is directly proportional to the experimentally calculated random motility coefficient ( $\mu$ ).

## DISCUSSION

The ability to engineer ligand-specific cell motility processes is critical in the control of motility of epithelial tissues on implanted biomaterials. Previously, we have examined the behavior of keratinocyte migration in the presence of a secondary, dynamic ligand interface and found that the induction of ligand-mediated phagocytic process via ligand-adsorbed microdepots significantly enhanced cell migratory responsiveness to the basal substrate ligand.<sup>33</sup> In this study, we have further investigated the rate governing mechanisms underlying this enhanced migration, via the development of a phenomenological model incorporating kinetic parameters for LAM binding and internalization.

Using the theoretical formalism developed in this study, we have tested the hypothesis that the internalizable nature of these ligand microdepots can differentially activate cell migration. Analysis of the rates of LAM binding and internalization shows that regardless of the initial LAM substrate density, (i) the rate of LAM binding is significantly greater than the rate of internalization, implying that the rate of LAM binding may be the primary migratory activation event in our system, and (ii) the rate of LAM binding quickly reaches a steady state, the exact level of which depends on the initial LAM density. In addition, further investigation suggests that keratinocyte motility may be differentially governed by the net equilibrium cell sampling rate of LAMs. Because the ligand concentration per microdepot is constant in our system,<sup>8</sup> the net rate of LAM sampling can be interpreted as the effective rate of accrued ligand on the cell surface, suggesting that migratory activity is an increasing function of the net rate of ligand sampling. Furthermore, our data indicate that regardless of the conditions

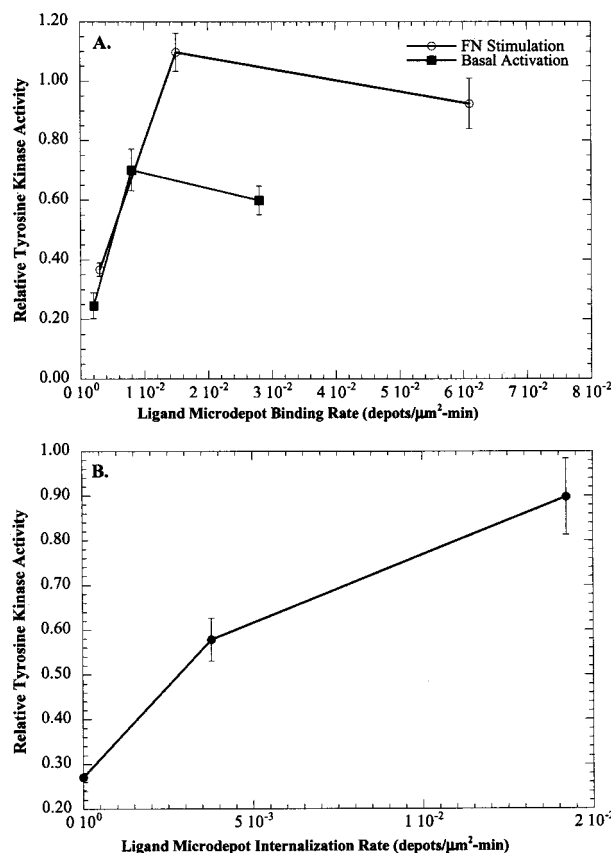


**FIGURE 10.** Effect of LAM binding, and internalization rates on cellular activation. (A) Effect of the relative tyrosine kinase activity on the LAM binding rate for both basal and fibronectin stimulated activation states. Tyrosine kinase activity values were obtained after cells were allowed to attach and migrate for 2 h, an early time point at which the rates of LAM internalization were not found to significantly vary with LAM substrate density. (B) Effect of LAM internalization rates on the relative tyrosine kinase activity. LAM internalization rates at the 2 h timepoint were found to significantly vary only with different activation states. Points were plotted from left to right for (i) covalently immobilized LAM, (ii) basal stimulated conditions, and (iii) fibronectin stimulated conditions. Binding, and internalization rates are theoretical values generated from model simulations. Tyrosine kinase activity values are the average of triplicate experimental samples from two experiments. The error bars represent the standard error.

of activation (e.g., basal activation or secondary stimulation by soluble fibronectin), the relationship between the ligand sampling rate and migratory activity remains qualitatively unchanged, suggesting that LAM-based activation due to different ligands (collagen versus fibronectin) may be fundamentally limited by the LAM sampling dynamics.

Previous studies on ligand-immobilized substrates have shown that ligand binding results in the activation of signal transduction pathways necessary for cell migration.<sup>3,9</sup> On ligand-immobilized substrates, for several cell types, the extent of activation of cell migration

can be primarily governed by the substrate adhesion strength, which quickly becomes inhibitory as the extent of ligand binding increases. By presenting the ligand via a dynamic, mobile microinterface, we hypothesize that we are able to significantly increase the “time-averaged” degree of ligand binding without significantly altering the cell–substrate adhesion strength necessary for migration, as reported recently.<sup>33</sup> Indeed, a 50-fold increase in the cell motility coefficient was elicited by LAMs relative to values for comparable concentrations of immobilized ligands.<sup>33</sup>

The ligand-specific internalization of LAMs is clearly central to the phagokinetic migration process. In fact, we have previously shown that cell migration is significantly impaired when LAM internalization processes are challenged via covalent conjugation of LAMs to the substrate.<sup>33</sup> It should also be noted that the direct contribution of internalization of “ligand-deficient microcarriers” to phagokinetic activation is rather small: our previous study quantified the ligand component to be the overwhelming ( $\sim 80\%$ ) component of the phagokinetic enhancement in migration.<sup>33</sup> We speculate that the internalization dynamics may enhance the time-averaged cell exposure to ligands by serving as an efficient means of ligand removal and receptor recycling. The rate of ligand internalization that may be necessary for optimal migration, then, would be dependent upon the rate of ligand binding and would be limited by the total number of receptors and amount of membrane available. Greater numbers of available receptors/membrane (modeled as “binding sites” in the model of this study) would result in the need for fewer recycled receptors/membrane to support the optimal rate of ligand binding, and thus would be consistent with activation via a slower rate of ligand internalization. Our simulations show that there is a time-based limitation on the kinetics of LAM internalization, presumably posed through carrier saturation intracellularly or at the membrane level. Indeed, the membrane/cytoskeletal limitation for LAM internalization is most intensified under conditions of highest LAM binding. Thus, for example, the internalization rate steadily decreased over time at the LAM density that promotes the greatest migration ( $1.21 \text{ LAMs}/\mu\text{m}^2$ ).

The LAM internalization can directly affect cytoskeletal processes, which are required for the generation of a sufficient traction force needed for migration. Since the collagen ligand density used in our studies ( $0.6 \mu\text{g}/\text{cm}^2$ ) (Ref. 32) is lower than that previously reported to be optimal for keratinocytes ( $3.7\text{--}4.4 \mu\text{g}/\text{cm}^2$ ),<sup>30,35</sup> in all of our studies herein, cell–substrate adhesion strength is low and, in the absence of LAMs, weak traction forces on the underlying substrate limit keratinocyte motility. The rate of LAM internalization may affect the degree of activation of the signal transduction pathways initiated by ligand binding. Increased levels of activation may

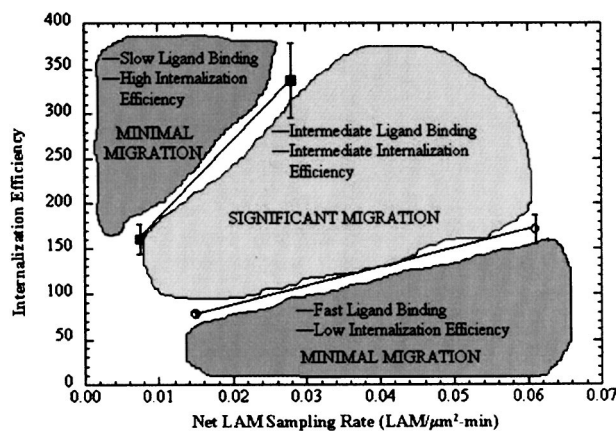


**FIGURE 11.** Map of internalization efficiency as a function of the rate of LAM binding. When the rate of LAM binding is relatively faster than the rate of internalization, activation efficiency of the internalization process is low and the extent of cell migration is minimal. Likewise, at relatively slow LAM binding rates compared to the internalization rate, where the majority of cellular activation is due to internalization, the efficiency of internalization is high, but migration is still minimal. In order to achieve significant levels of migration, an intermediate rate of LAM binding and LAM internalization are necessary.

generate sufficient cellular contractile forces to overcome weak cell adhesion to the substrates. In fact, previous investigations into the temporal coordination between the forces within the cell cytostructure and cell spreading during phagocytosis have shown that phagocytic ingestion results in the generation of a significant cell contractile force that is critically dependent upon the accumulation of tyrosine phosphoproteins.<sup>13,26</sup> Pseudopod extension and binding, on the other hand, do not appear to necessarily require tyrosine kinase activity.<sup>26</sup> Our own studies examining the net tyrosine kinase (ntk) activity of migrating keratinocytes show that at higher values of LAM binding rates, ntk activity does not change much, whereas as LAM internalization rates are increased, ntk activity increases monotonically. Thus, as the net LAM sampling rate increases, the proportion of ntk activity due to LAM internalization relative to that arising from LAM binding, increases. A plot of parameter  $\varepsilon_i$  (defined as cell activation normalized to LAM internalization rate) versus the LAM sampling rate permits a mapping of regions of low and high levels of cell migration in the context of rates of LAM binding and internalization (Fig. 11). When the LAM binding rate is relatively fast compared to the internalization rate,  $\varepsilon_i$  will be low and the extent of cell migration observed is minimal. Likewise, at relatively high internalization rates and low LAM binding rates, the amount of activation due to internalization is high, but migration is still minimal. We propose that in order to achieve significant amounts of migration, cellular activation must be engendered via

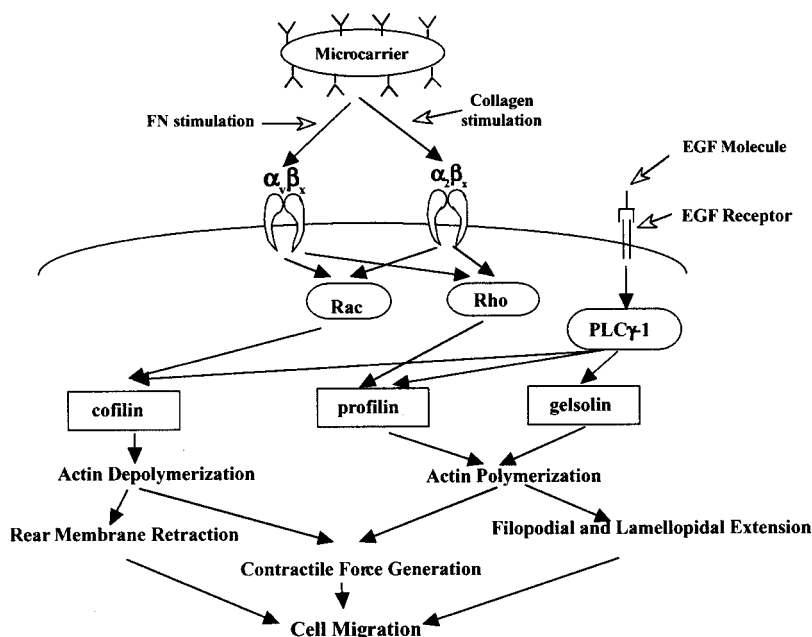


**FIGURE 12.** Intracellular signal activation pathways due to internalizable ligand associated microdepots. We propose that exogenous ligand binding to LAMs followed by LAM internalization may activate cell migration by cooperative intensification of the native signaling pathways resulting from ligand–receptor binding and internalization mediated by phagocytic integrin receptors. For example, membrane ligation and internalization of integrin receptors leads to the activation of rac and rho (Ref. 24), which ultimately leads to the polymerization and depolymerization of actin stress fibers (Refs. 6 and 10). Stimulation with soluble fibronectin enables utilization of integrin receptors in addition to collagen specific integrins, further stimulating the rac and rho pathways. While LAM binding primarily activates pathways used for the pseudopod extension and retraction, LAM internalization serves to activate pathways necessary for the generation of a contractile force. Notably, LAMs intensify migration in the presence of EGF, indicating overlap between EGF receptor induced alterations in the actin cytoskeleton.

critical rates of both LAM binding and internalization, which likely activate pathways leading to pseudopod extension and retraction, and the generation of a bulk contractile force, respectively.<sup>10,26</sup> Based on the current knowledge in the field, the cartoon in Fig. 12 depicts the possible interactions between LAM binding/internalization, and the intracellular molecular signaling targets that can govern enhanced levels of cell migration. In the future, more mechanistic efforts will be required to distinguish the effects of LAM trafficking dynamics on individual signaling/protein targets. The current phenomenological study provides the framework to conduct such studies.

In conclusion, we have examined the roles of microdepot binding and internalization on the activation of the enhanced cellular migration observed on substrates containing ligand-adsorbed microdepots. Our analysis indicated that the extent of migration is differentially controlled by the rates of LAM binding and internalization. We propose that there exists a regime in which the use of ligand microdepots results in an optimal balance between the extent of activation due to LAM binding and that due to LAM internalization, leading to enhanced migration. The results of these studies may aid in the design of biomimetic strategies for directed cell migration on biomaterials used in tissue-engineered systems and may also

have implications for applications involving rapid ligand based biosensing.<sup>22</sup>

## ACKNOWLEDGMENTS

This study was supported by Johnson & Johnson Discovery Award, ConvaTec Young Professor Award, and Hoechst Celanese Innovative Research Award to P. Moghe. The authors would like to thank Howard Salis, a NJ Center for Biomaterials Summer Fellow, and Patrick Hossler for their help with image analysis. One of the authors (J.S.T.) was partially supported by the Rutgers–UMDNJ National Institutes of Health Biotechnology Training Grant, and the Rutgers University Louis Bevier Fellowship.

## REFERENCES

- Albrecht-Buehler, G. The phagokinetic tracks of 3T3 cells. *Cell* 11:395–404, 1977.
- Albrecht-Buehler, G., and M. M. Yarnell. A quantitation of movement of marker particles in the plasma membrane of 3T3 mouse fibroblasts. *Experimental methods. Exp. Cell Res.* 78:67–70, 1973.
- Asthagiri, A. R., C. M. Nelson, A. F. Horwitz, and D. A. Lauffenburger. Quantitative relationship among integrin–

- ligand binding, adhesion, and signaling via focal adhesion kinase and extracellular signal-regulated kinase 2. *J. Biol. Chem.* 274:27119–27127, 1999.
- <sup>4</sup>Beumer, G. J., C. A. Van Blitterswijk, D. Bakker, and M. Ponc. Cell seeding and *in vitro* biocompatibility evaluation of polymeric matrices of PEO/PBT copolymers and PLLA. *Biomaterials* 14:598–604, 1993.
- <sup>5</sup>Cannon, G. J., and J. A. Swanson. The macrophage capacity for phagocytosis. *J. Cell. Sci.* 101:907–913, 1992.
- <sup>6</sup>Carlier, M.-F., and D. Pantaloni. Control of actin dynamics in cell motility. *J. Mol. Biol.* 269:459–467, 1997.
- <sup>7</sup>The Molecular and Cellular Biology of Wound Repair, 2nd ed., edited by R. A. F. Clark. New York: Plenum, 1996.
- <sup>8</sup>De Roe, C., P. J. Courtoy, and P. Baudhuin. A model for protein–colloidal gold interactions. *J. Histochem. Cytochem.* 35:1191–1198, 1987.
- <sup>9</sup>Dedhar, S., and G. E. Hannigan. Integrin cytoplasmic interactions and bidirectional transmembrane signaling. *Curr. Opin. Cell Biol.* 8:657–669, 1996.
- <sup>10</sup>Defilippi, P., C. Olivo, M. Venturino, I. Dolce, L. Silengo, and G. Tarone. Actin cytoskeleton organization in response to integrin-mediated adhesion. *Microsc. Res. Tech.* 47:67–78, 1999.
- <sup>11</sup>DiMilla, P. A., K. Barbee, and D. A. Lauffenburger. Mathematical model for the effects of adhesion and mechanics on cell migration speed. *Biophys. J.* 60:15–37, 1991.
- <sup>12</sup>Dunn, G. A. Characterizing a kinesis response: Time-averaged measures of cell speed and directional persistence. *Agents Actions Suppl.* 12:14–33, 1983.
- <sup>13</sup>Evans, E., A. Leung, and D. Zhelev. Synchrony of cell spreading and contraction force as phagocytes engulf large pathogens. *J. Cell Biol.* 122:1295–1300, 1993.
- <sup>14</sup>Farrell, B. E., R. P. Daniele, and D. A. Lauffenburger. Quantitative relationships between single-cell and cell-population model parameters for chemosensory migration responses of alveolar macrophages to C5a. *Cell Motil. Cytoskeleton* 16:279–293, 1990.
- <sup>15</sup>Gail, M., and C. Boone. The locomotion of mouse fibroblasts in tissue culture. *Biophys. J.* 10:980–993, 1970.
- <sup>16</sup>Green, H. Cultured cells for the treatment of disease. *Sci. Am.* 265:96–102, 1991.
- <sup>17</sup>Griffin, F. M., J. A. Griffin, J. E. Leider, and S. C. Silverstein. Studies of the mechanism of phagocytosis. I. Requirements for circumferential attachment of particle-bound ligands to specific receptors on the macrophage plasma membrane. *J. Exp. Med.* 142:1263–1282, 1975.
- <sup>18</sup>Griffin, F. M., J. A. Griffin, and S. C. Silverstein. Studies on the mechanism of phagocytosis. II. The interactions of macrophages with anti-immunoglobulin IgG-coated bone marrow-derived lymphocytes. *J. Exp. Med.* 144:788–809, 1976.
- <sup>19</sup>Griffin, F. M., and S. C. Silverstein. Sequential response of the macrophage plasma membrane to a phagocytic stimulus. *J. Exp. Med.* 139:323–336, 1974.
- <sup>20</sup>Griffith, L. G., and S. T. Lopina. Microdistribution of substratum-bound ligands affects cell function: Hepatocyte spreading on PEO-tethered galactose. *Biomaterials* 19:979–986, 1998.
- <sup>21</sup>Grinnell, F. Fibroblast receptor for cell–substratum adhesion: Studies on the interaction of baby hamster kidney cells with latex beads coated by cold insoluble globulin (plasma fibronectin). *J. Cell Biol.* 86:104–112, 1980.
- <sup>22</sup>Guertens, G., K. Van Cauwenberghe, D. B. G., R. Maes, U. R. Tjaden, J. Van der Greef, M. Highley, A. T. van Oosterm, and E. A. de Bruijn. Nanotechnology in bio/clinical analysis. *J. Chromatogr., B: Biomed. Sci. Appl.* 739:139–150, 2000.
- <sup>23</sup>Hammer, D. A., and M. Tirrell. Biological adhesion at interfaces. *Polymers Ann. Rev. Mater. Sci.* 26:651–691, 1996.
- <sup>24</sup>Kjoller, L., and A. Hall. Signaling to Rho GTPases. *Exp. Cell Res.* 253:166–179, 1999.
- <sup>25</sup>Lauffenburger, D. A., and A. F. Horwitz. Cell Migration: A physically integrated process. *Cell* 84:359–369, 1996.
- <sup>26</sup>Lowry, M. B., A.-M. Duchemin, J. M. Robinson, and C. L. Anderson. Functional separation of pseudopod extension and particle internalization during Fc $\gamma$  receptor-mediated phagocytosis. *J. Exp. Med.* 187:161–176, 1998.
- <sup>27</sup>McAbee, D. D., and F. Grinnell. Fibronectin-mediated binding and phagocytosis of polystyrene latex beads by baby hamster kidney cells. *J. Cell Biol.* 97:1515–1523, 1983.
- <sup>28</sup>Othmer, H. G., S. R. Dunbar, and W. Alt. Models of dispersal in biological systems. *J. Math. Biol.* 26:263–298, 1988.
- <sup>29</sup>Rabinovitch, M. Professional and nonprofessional phagocytes: An introduction. *Trends Cell Biol.* 5:85–87, 1995.
- <sup>30</sup>Sarret, Y., D. T. Woodley, K. Grigsby, K. Wynn, and E. J. O'Keefe. Human keratinocyte locomotion: The effect of selected cytokines. *J. Invest. Dermatol.* 98:12–16, 1992.
- <sup>31</sup>Stenn, K. S., R. Link, G. Moellmann, J. Madri, and E. Kukulinska. Dispase, a neutral protease from *Bacillus polymyxa*, is a powerful fibronectinase and type IV collagenase. *J. Invest. Dermatol.* 93:287–290, 1989.
- <sup>32</sup>Tjia, J. S., B. J. Aneskievich, and P. V. Moghe. Substrate-adsorbed collagen and cell-secreted fibronectin concertedly induce cell migration on poly(lactide–glycolide) substrates. *Biomaterials* 20:2223–2233, 1999.
- <sup>33</sup>Tjia, J. S., and P. V. Moghe. Regulation of cell motility on polymer substrates via “dynamic,” cell internalizable, ligand microinterfaces. *Tissue Eng.* 8:247–259, 2002.
- <sup>34</sup>Webb, K., V. Hlady, and P. A. Tresco. Relationships among cell attachment, spreading, cytoskeletal organization, and migration rate for anchorage-dependent cells on model surfaces. *J. Biomed. Mater. Res.* 49:362–368, 2000.
- <sup>35</sup>Woodley, D. T., P. M. Bachmann, and E. J. O'Keefe. Laminin inhibits human keratinocyte migration. *J. Cell Physiol.* 136:140–146, 1988.